www.acsnano.org

## This article is licensed under CC-BY-NC-ND 4.0 (cc) (\*) (\$ (=)

# Nanotopographical Cues Tune the Therapeutic Potential of Extracellular Vesicles for the Treatment of Aged Skeletal Muscle **Injuries**

Kai Wang,\* Nolan Frey, Andres Garcia, Kun Man, Yong Yang, Alice Gualerzi, Zachary J. Clemens, Marzia Bedoni, Philip R. LeDuc, and Fabrisia Ambrosio\*



Cite This: ACS Nano 2023, 17, 19640-19651



**ACCESS** 

See https://pubs.acs.org/sharingguidelines for options on how to legitimately share published articles.

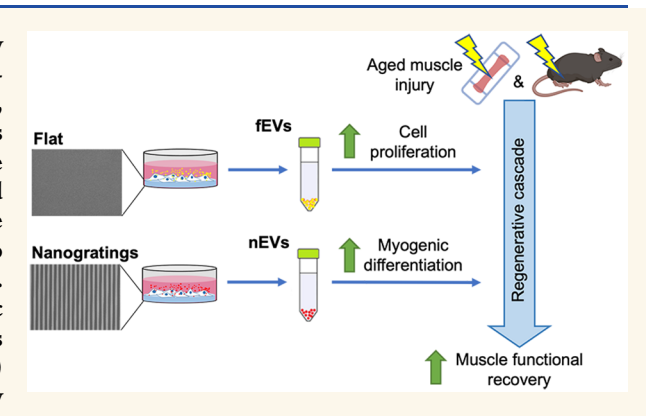
Downloaded via 24.239.46.20 on June 21, 2024 at 13:51:00 (UTC).

III Metrics & More

Article Recommendations

s Supporting Information

ABSTRACT: Skeletal muscle regeneration relies on the tightly temporally regulated lineage progression of muscle stem/progenitor cells (MPCs) from activation to proliferation and, finally, differentiation. However, with aging, MPC lineage progression is disrupted and delayed, ultimately causing impaired muscle regeneration. Extracellular vesicles (EVs) have attracted broad attention as next-generation therapeutics for promoting tissue regeneration. As a next step toward clinical translation, strategies to manipulate EV effects on downstream cellular targets are needed. Here, we developed an engineering strategy to tune the therapeutic potential of EVs using nanotopographical cues. We found that EVs released by young MPCs cultured on flat substrates (fEVs) promoted the proliferation of aged MPCs while EVs released by MPCs cultured on nanogratings (nEVs) promoted myogenic



differentiation. We then employed a bioengineered 3D muscle aging model to optimize the administration protocol and test the therapeutic potential of fEVs and nEVs in a high-throughput manner. We found that the sequential administration first of fEVs during the phase of MPC proliferative expansion (i.e., 1 day after injury) followed by nEV administration at the stage of MPC differentiation (i.e., 3 days after injury) enhanced aged muscle regeneration to a significantly greater extent than fEVs and nEVs delivered either in isolation or mixed. The beneficial effects of the sequential EV treatment strategy were further validated in vivo, as evidenced by increased myofiber size and improved functional recovery. Collectively, our study demonstrates the ability of topographical cues to tune EV therapeutic potential and highlights the importance of optimizing the EV administration strategy to accelerate aged skeletal muscle regeneration.

**KEYWORDS:** cell-free therapy, exosomes, aging, skeletal muscle repair, nanotopography

#### **INTRODUCTION**

Skeletal muscle regeneration is a complex, yet effective, process that relies on the activity of muscle stem/progenitor cells (MPCs). During muscle regeneration, MPCs undergo a carefully orchestrated lineage progression, advancing from quiescence to activation, proliferation, and myogenic differentiation to form myofibers.<sup>1,2</sup> However, with aging, MPC responses at each of these stages become compromised,<sup>3-5</sup> ultimately resulting in diminished muscle regeneration.<sup>2,3</sup> Cellbased strategies, such as cell transplantation, have been pursued to boost skeletal muscle repair in the setting of disease or aging.<sup>6–8</sup> For example, transplantation of young or rejuvenated aged MPCs improved the repair of aged muscle

after acute injuries.9 Yet, despite the promising outcomes, clinical applications of cell-based strategies have been limited because in vitro cell expansion usually results in a significant reduction of cellular regenerative capacity. 10,11 As such, increased attention has been given to isolating the proregenerative effects of cellular therapies while mitigating the

Received: March 10, 2023 Accepted: September 22, 2023 Published: October 5, 2023





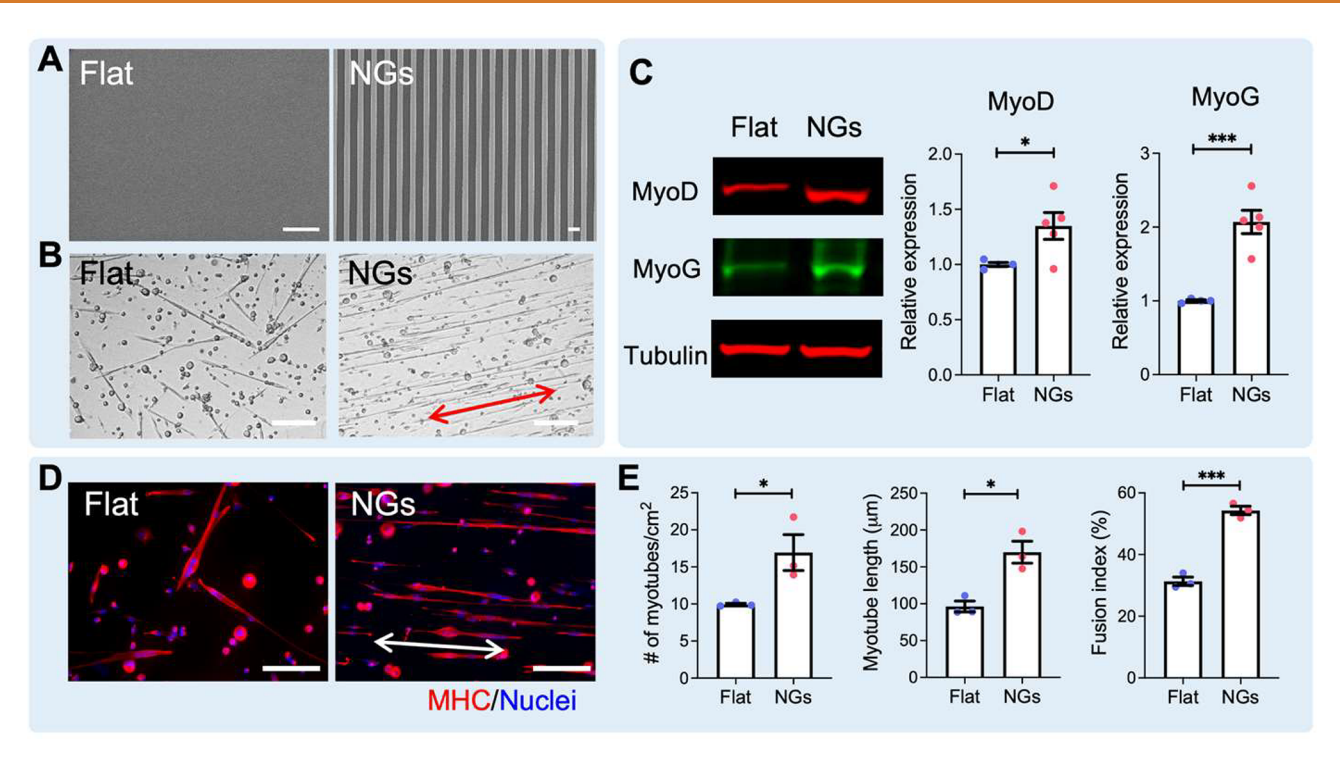


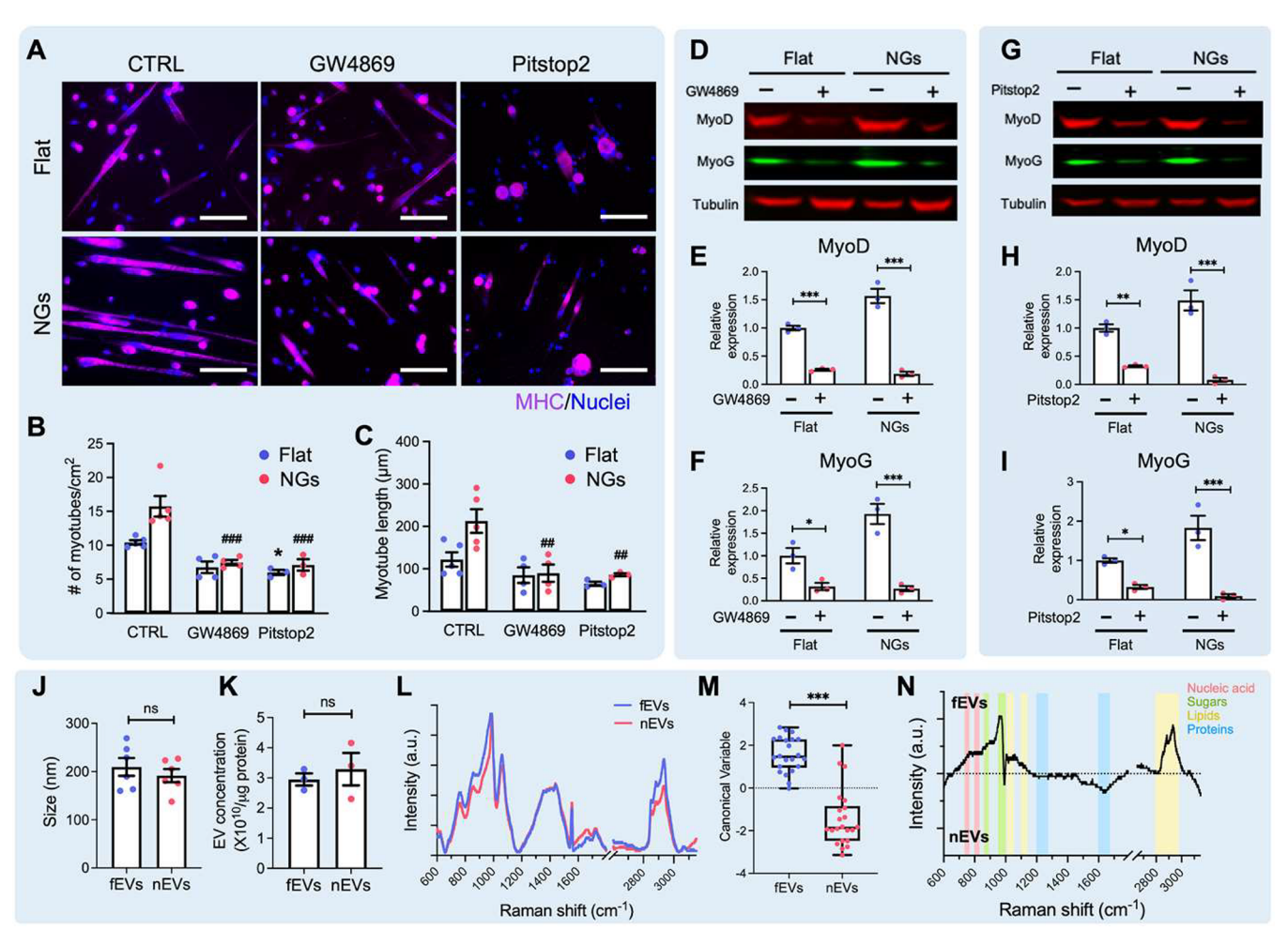
Figure 1. Nanogratings promoted myogenic differentiation of young MPCs. (A) Scanning electron microscope micrographs of PDMS flat substrate (Flat) and nanogratings (NGs). Scale bars = 1  $\mu$ m. (B) Morphology of MPCs and myotubes on flat and nanograting substrates. The red arrow indicates the nanograting direction. Scale bars = 100  $\mu$ m. (C) Western blot analysis of MyoD and MyoG expression in MPCs cultured on flat or nanograting substrates. \*p < 0.05, \*\*\* p < 0.001, two-tailed Student's t test (n = 4–5). (D) Immunofluorescent images of myotubes stained for MHC (red), nuclei (DAPI; blue). The white arrow indicates the nanograting direction. Scale bars = 100  $\mu$ m. (E) Quantification of the relative number, length, and fusion index of myotubes formed by MPCs on flat and nanograting substrates. The myotube fusion index is defined as the percentage of nuclei inside the myotubes. \*p < 0.05, \*\*\* p < 0.001, two-tailed Student's t test (n = 3). Data are presented as means  $\pm$  SEM.

limitations. To this end, growing evidence has shown that a large portion of the beneficial effects of transplanted cells are mediated by paracrine factors, <sup>12,13</sup> suggesting that harnessing these paracrine factors may be a promising alternative to cell transplantation.

Among such paracrine factors, extracellular vesicles (EVs) demonstrate encouraging potential to promote tissue regeneration. 14 EVs are membrane-bound vesicles that are secreted by almost all types of cells.<sup>15</sup> EVs contain molecular information in the form of proteins, lipids, and nucleic acids that can be transferred to recipient cells to direct cellular responses and behavior. 16 The ability of EVs to efficiently transfer their cargo to recipient cells makes EVs a promising cell-free therapeutic tool in regenerative medicine. For instance, EVs released by different types of stem cells such as mesenchymal stem cells (MSCs) and MPCs promote the regeneration of a wide variety of tissues, including skin, bone, and skeletal muscle. 17-19 Furthermore, studies have shown that the therapeutic potential of EVs is dependent on their molecular cargoes, which are closely associated with the phenotype of the originating cell source. <sup>19–21</sup> For example, EVs released by differentiating, but not proliferating, human MPCs improved skeletal muscle regeneration of the 5-week-old mice.<sup>19</sup> Therefore, when generating functional EVs, modulation of the originating cell phenotype represents a promising approach to manipulate EV therapeutic performance.

Inspired by nanoscale architectural characteristics of the native extracellular matrix, substrates fabricated with varying nanotopographies have been pursued by a number of groups to control cell behavior for tissue engineering and regenerative medicine. <sup>22–24</sup> Nanogratings or aligned nanofibers have been widely used to induce alignment and differentiation of MSCs or myoblasts to drive myotube formation *in vitro* and promote muscle regeneration *in vivo*. <sup>25–27</sup> While most of these studies focused on investigating how nanotopographical cues directly influence cellular responses, few have explored the potential effects of nanotopography on EV biomolecular cargoes. <sup>28,29</sup>

In this study, we used nanotopographical cues to tune the therapeutic potential of EVs for the treatment of aged skeletal muscle injury. We demonstrated that nanogratings promoted MPC myogenic differentiation and myotube formation, consistent with previous studies. 30,31 We further showed that the enhanced myogenic differentiation of cells on nanotopological substrates was dependent on EV secretion and uptake. When we directly compared the downstream effects of EVs isolated from young MPCs cultured on flat surfaces (fEVs) versus nanogratings (nEVs), we found that each EV population elicited distinct effects on recipient aged cells. That is, fEVs preferentially enhanced aged MPC proliferation while nEVs promoted myogenic differentiation. We then leveraged this information to optimize the delivery and timing of fEVs and nEVs using a high-throughput bioengineered 3D muscle aging model. We found that only sequential administration first of fEVs then nEVs improved muscle regeneration in the engineered muscles. Our protocol was further validated in vivo using aged mice, in which aged mice treated with fEVs during the phase of MPC proliferative expansion followed by nEVs during the phase of differentiation displayed improved



functional regeneration to levels comparable to young counterparts.

## **RESULTS AND DISCUSSION**

Nanogratings Promoted the Myogenic Differentiation of Young MPCs. Myofibers within skeletal muscle are highly aligned, facilitating the production of contractile forces while also providing contact guidance for MPC division. To mimic this *in vivo* aligned fiber feature, we fabricated nanogratings on PDMS substrates (Figure 1A) to induce alignment and elongation of MPCs. Engineered nanogratings were  $500 \pm 13$  nm in line width,  $648 \pm 28$  nm in spacing, and  $631 \pm 50$  nm in height. This feature size of nanogratings was selected based on our previous studies, which demonstrated that nanogratings of similar dimensions were the most efficient in modulating cell proliferation and differentiation when compared to flat substrates. Moreover, previous studies

have shown that nanogratings of similar feature sizes promoted myogenic differentiation of both primary and immortalized myoblasts. <sup>30,31</sup>

We first confirmed the influence of nanogratings on MPC phenotype. Young MPCs isolated from 3 to 5-month-old male mice were cultured on nanogratings or flat PDMS substrates for 3 days. As shown in Figure 1B, MPCs and formed myotubes were randomly oriented when seeded on flat surfaces, while myotubes were aligned along the direction of the nanogratings. Nanogratings also significantly increased the expression of MyoD and Myogenin (MyoG), master regulatory proteins of myogenesis, when compared to flat controls (Figure 1C). These data confirmed that nanogratings promoted MPC myogenicity.

We then compared myotube formation across groups by staining cells for myosin heavy chain (MHC). Compared to flat substrates, nanogratings enhanced the formation of

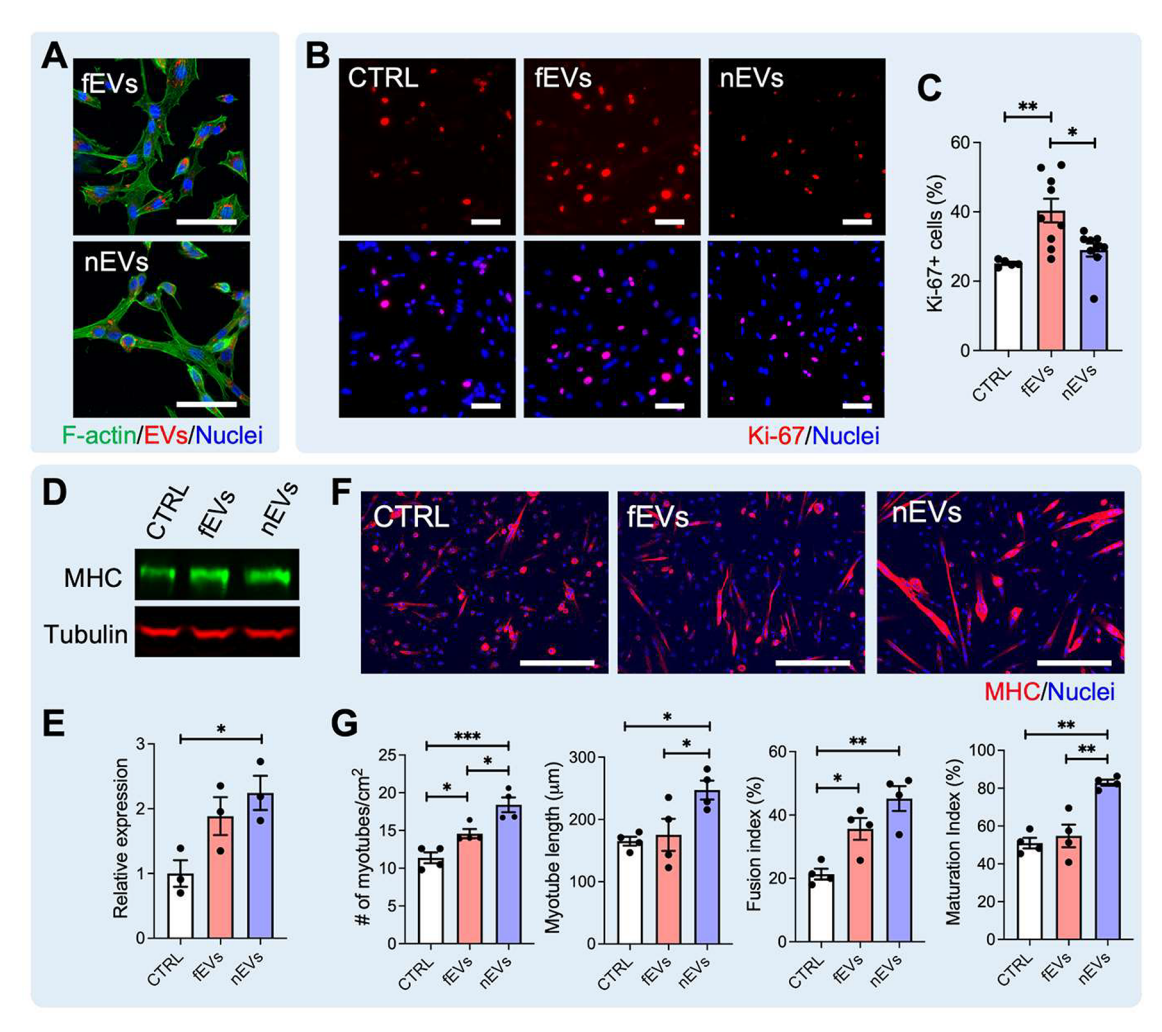


Figure 3. Cell substrates modulated the function of MPC-derived EVs. (A) EV uptake by aged MPCs. EVs were labeled by PKH26 in red. Cells were stained by phalloidin in green. Blue: nuclei. Scale bar: 50  $\mu$ m. (B) Representative fluorescence images and (C) quantification of Ki-67 positive aged MPCs after EV treatment. CTRL: no treatment. Red: Ki-67; blue: nuclei. Scale bar: 50  $\mu$ m. \* p < 0.05, \*\* p < 0.01, Oneway ANOVA. (n = 5-9). (D) Western blot analysis and (E) quantification of MHC expression in MPCs after EV treatment. \* p < 0.05, Oneway ANOVA. (n = 3). (F) Representative fluorescence images and (G) quantification of myotubes formed by age MPCs after EV treatment. The maturation index is defined as the percentage of myotubes containing more than five nuclei. Magenta: MHC; Blue: Nuclei. Scale bar:  $100 \ \mu$ m. \* p < 0.05, \*\* p < 0.01, \*\*\* p < 0.001, nonparametric ANOVA (myotube number) and one-way ANOVA (myotube length, fusion index, and maturation index) (n = 4). Data are presented as means  $\pm$  SEM.

myotubes, as evidenced by increased myotube number, length, and fusion index (Figure 1D,E). Furthermore, we found that nanogratings promoted the expression and phosphorylation of p38 mitogen-activated protein kinases (MAPK) (Figure S1). P38 MAPK plays a crucial role in cell mechanotransduction and its activation is required for cell myogenesis. Previous work showed that discrete nanorods inhibited the expression of p38 MAPK in C2C12 myoblasts and attenuated cell fusion, a coordance with our current finding. Overall, our results suggest that, compared to cells seeded on flat substrates, nanogratings promoted myogenic differentiation of young MPCs and facilitated myotube formation.

Substrate Nanotopography Altered the Biochemical Composition of MPC-Derived EVs. Next, we sought to determine whether the effects of substrate nanotopography on MPC responses were mediated by the function of EVs. For this, young MPCs cultured on nanogratings or flat surfaces were treated with either GW4869 or Pitstop2 to inhibit EV biogenesis and uptake, respectively. GW4869, a neutral sphingomyelinase inhibitor, inhibits the release of mature

exosomes from multivesicular bodies.<sup>39</sup> Pitstop2 blocks clathrin-dependent endocytosis of EVs.<sup>40</sup> As shown in Figure 2A–C, nanograting-induced myotube formation was significantly blunted by GW4869, as evidenced by reduced myotube number and length after GW4869 treatment. Similarly, inhibiting cellular uptake of EVs attenuated myotube formation (Figure 2A–C). Furthermore, both MyoD and MyoG expression were significantly reduced in the cells treated with GW4869 or Pitstop2 (Figure 2D–I). Previous work showed that GW4869 or heparin treatment (to inhibit exosome generation and uptake, respectively) reduced the myogenic differentiation and myotube formation of C2C12 myoblasts, in agreement with our current findings.<sup>41</sup> Overall, our results indicate that EVs play a critical role in MPC myogenesis and nanograting-mediated myotube formation.

Studies have shown that nanorough surfaces enhanced the ability of MSC-derived EVs to induce osteogenesis *in vitro* and *in vivo*, suggesting the potential effects of nanotopography on EV function. Therefore, As the next step to investigate whether nanogratings affected the profile and function of EVs

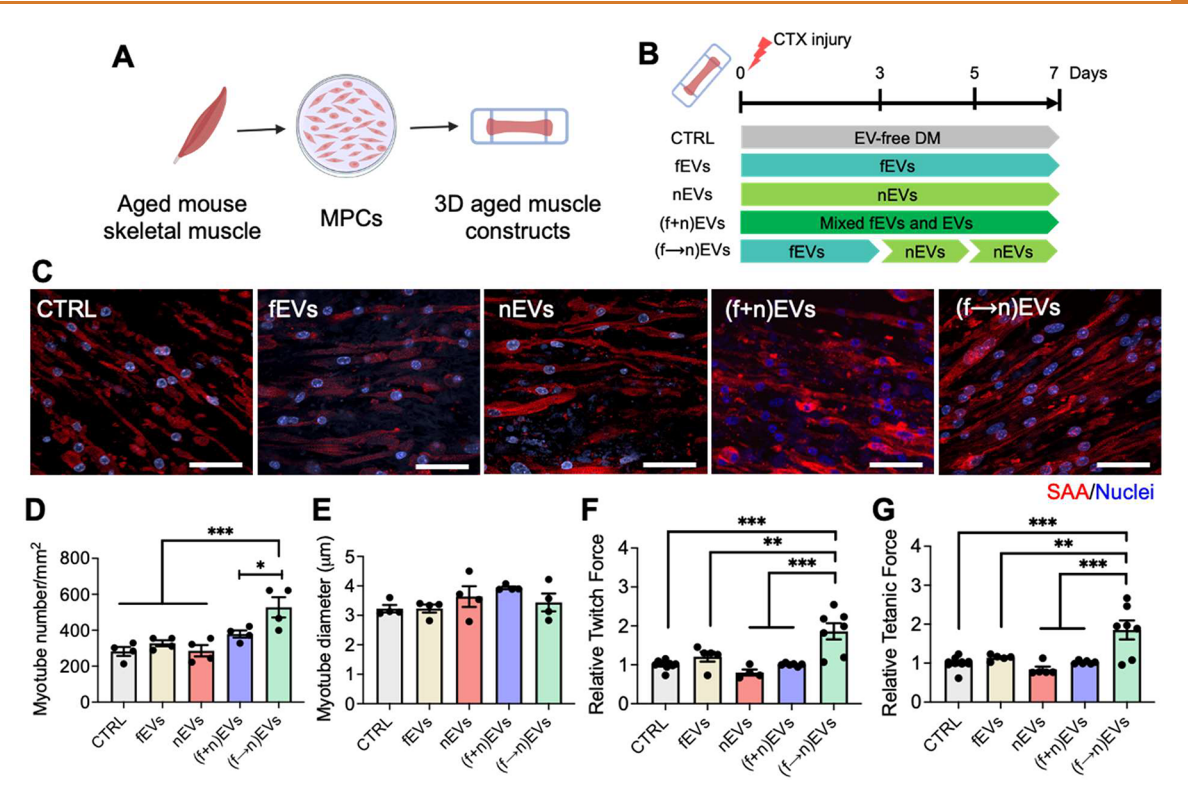


Figure 4. Optimization of EV treatment strategies using bioengineered aged muscle constructs. (A) Schematic illustration of 3D muscle construct preparation. (B) Schematic illustration of EV administration strategies and timeline. Aged muscle constructs were injured by CTX, followed by EV treatments for a total of 7 days. At 7 DPI, myotube regeneration and muscle construct force recovery were evaluated. In control group (CTRL), injured muscle constructs were cultured in EV-free differentiation media (DM). (C) Representative confocal images of injured muscle constructs (7 DPI) stained for sarcomeric  $\alpha$ -actinin (SAA) to show myotube regeneration without or with EV treatment. Red: SAA; blue: nuclei. Scale bar = 100  $\mu$ m. (D) Quantification of myotube number and (E) myotube diameter of injured muscle constructs without or with the EV treatment at 7 DPI. \* p < 0.05, \*\*\* p < 0.001, one-way ANOVA. (n = 4) (F, G) Relative twitch and tetanic forces of injured muscle constructs (7 DPI) without or with EV treatment. Force data were normalized to the CTRL group. \*\*\* p < 0.01, \*\*\*\* p < 0.001, one-way ANOVA. (n = 4-10). Data are presented as means  $\pm$  SEM.

secreted by MPCs, we cultured young MPCs in EV-free media for 3 days on either nanogratings or flat surfaces. We then isolated EVs from the conditioned media of the different groups. The abbreviations, fEVs and nEVs are used to represent EVs secreted by young MPCs cultured on flat and nanograting substrates, respectively. Nanoparticle tracking analysis showed that both fEVs and nEVs had an average diameter of ~200 nm, suggesting substrate topology did not affect the EV size (Figure 2J). The concentration of EVs secreted by MPCs was also not significantly changed by the substrate nanotopography (Figure 2K). Both fEVs and nEVs were positive for CD81 and Alix, two EV-specific markers, and negative for cytoplasmic protein GM130 (Figure S2).

To gain insights into the influences of nanotopography on EV biochemical composition, we used Raman spectroscopy analysis to compare the fEVs and nEVs molecular fingerprints, including protein, nucleic acid, lipid, and sugar content. EV Raman fingerprints mirror the biochemical features and health status of the parental cell and contain information about the structural and functional components of the EVs. As shown in Figure 2L, the obtained Raman spectra displayed a good signal-to-noise ratio and showed the peaks and bands that were expected for EV components (lipids, proteins, nucleic acids, and sugars). Multivariate statistical analysis of the observed spectral variations indicated that fEVs and nEVs had significant differences in their biochemical composition (Figure 2M). We further compared the levels of different EV components and

found that nEVs displayed reduced levels of lipid and sugar compositions when compared to fEVs, while the protein and nucleic acid contents were only modestly changed between the two EV types (Figure 2N). Studies have shown that nanotopographical signals regulate cell lipid metabolism and the membrane distribution of bulky glycoproteins, 45,46 which may contribute to the nanograting-modulated changes in EV lipid and sugar compositions. However, further investigation is required to understand the specific EV molecular changes in response to substrate topographical cues. Overall, these results suggest that the molecular signals contained within EVs are modulated by changing the physical features of cell culture substrates from which the EVs originated.

**fEVs and nEVs Play a Distinct Role in Modulating Aged MPC Behavior.** To assess the direct effect of fEVs and nEVs on aged MPC responses, we isolated MPCs from the hindlimb muscles of aged male mice (21–23-month-old) and treated aged MPCs with fEVs or nEVs. Immunofluorescent labeling confirmed that EVs were taken up by cells 4 h after treatment (Figure 3A). As aging induces the impairment of MPC proliferation and differentiation potentials, <sup>4,47,48</sup> we focused on evaluating the roles of fEVs and nEVs in regulating these two features in aged MPCs. After 24 h of treatment, fEVs increased the percentage of proliferating cells (Ki-67 positive) compared to both nEVs and no treatment controls (Figure 3B,C). Cell proliferation was not significantly influenced by the presence of nEVs. These results were further confirmed using

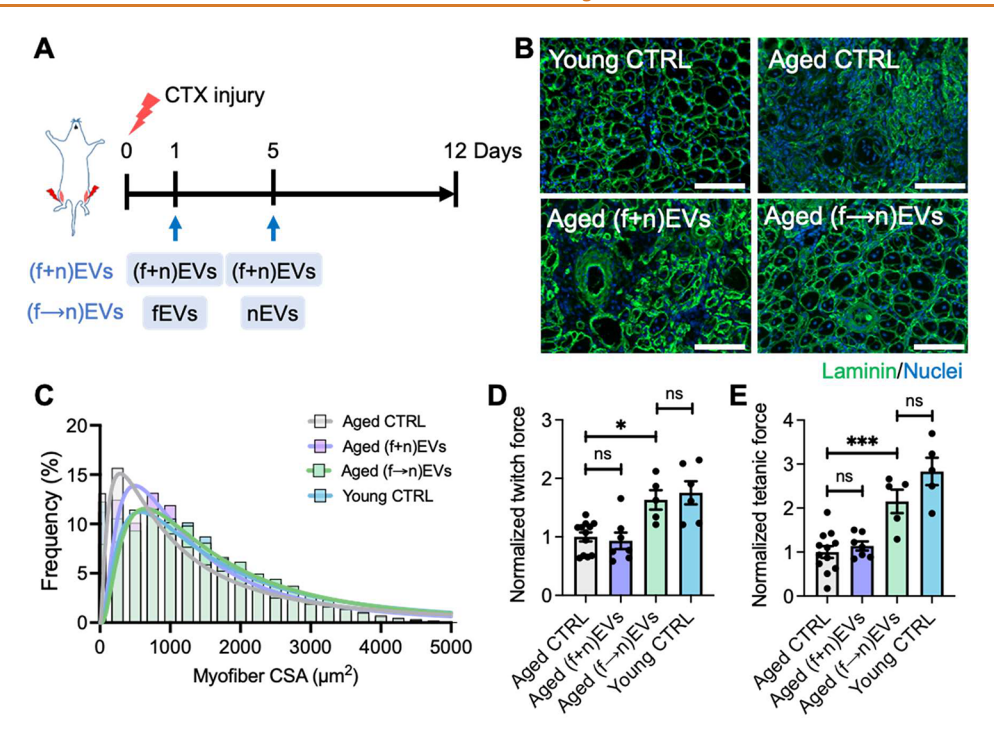


Figure 5. Sequential administration of fEVs and nEVs enhanced aged muscle regeneration in vivo. (A) Schematic illustration of EV administration. (B) Representative cross-sectional images of injured TA muscles (12 DPI) with or without EV treatment. Young CTRL: injured TA muscles of young mice injected with PBS; Aged CTRL: injured TA muscles of aged mice injected with PBS; (f+n)EVs: injured TA muscles of aged mice injected with an EV mixture containing  $5 \times 10^8$  fEVs and  $5 \times 10^8$  nEVs at both 1 and 5 DPI;  $(f \rightarrow n)$ EVs: injured TA muscles of aged mice injected with fEVs  $(1 \times 10^9)$  and nEVs  $(1 \times 10^9)$  at 1 and 5 DPI, respectively. Green: laminin; blue: nuclei. Scale bar =  $100 \, \mu$ m. (C) Size distribution of myofibers of injured TA muscles with or without EV treatment (n = 5 - 6). (D) Relative twitch and (E) tetanic force of TA muscles with or without EV treatment (12 DPI). Force data were normalized to the aged CTRL group. \* p < 0.05, \*\*\* p < 0.001, ns: no significance, one-way ANOVA (n = 5 - 12). Data are presented as means  $\pm$  SEM.

an MTS (3-(4,5-dimethylthiazol-2-yl)-5-(3-carboxymethoxyphenyl)-2-(4-sulfophenyl)-2H-tetrazolium) assay (Figure S3). We then evaluated the myogenic differentiation of aged MPCs that were treated with fEVs or nEVs for 3 days. As shown in Figure 3D,E, nEV treatment significantly increased MHC expression in the cells when compared to the no treatment control cells. We also observed that fEVs increased MHC expression, although the increase was not statistically significant. This increase may be due to fEVs-induced increase in cell number, which would result in enhanced cell-cell contact and, thus, myogenesis. 49,50 Indeed, fEV treatment increased the number of myotubes and the fusion index in MPCs compared to control cells (Figure 3F,G). However, myotubes were generally small, with ~50% of the myotubes containing less than 5 nuclei (Figure 3F,G). By comparison, nEVs significantly increased the numbers of myotubes, myotube length, and myotube maturation as compared to both control and fEVs groups (Figure 3F,G). Taken together, our results suggest that fEVs and nEVs display distinct effects in mediating aged MPC behavior, which may result from nanotopography-induced EV composition change.

A Bioengineered Muscle Aging Model Identified an Optimal EV Administration Protocol for Improved Functional Muscle Regeneration. Having demonstrated the capabilities of both fEVs and nEVs in mediating different aspects of aged MPCs lineage progression, we next tested whether one or both of these EV populations could enhance aged muscle regeneration *in vivo*. Tibialis anterior (TA) muscles of aged mice were injured by cardiotoxin (CTX), then received local administration of fEVs or nEVs 5 and 7 days

after injury, similar to our previous protocol.<sup>51</sup> However, we found that neither the administration of fEVs nor the administration of nEVs significantly improved the regeneration of aged muscles when compared to controls (Figure S4).

Since aged MPCs display impairment in both proliferation and differentiation,<sup>3–5</sup> we posited that the failure of fEVs or nEVs to promote functional regeneration *in vivo* might be because neither EV population in isolation promotes multiple phases of MPC lineage progression. That is, while fEVs may have promoted MPC proliferation, differentiation potential in the later stages of regeneration was unaffected. In contrast, nEVs may have precociously promoted MPC differentiation before MPCs were sufficiently amplified in number. Previous studies have shown that this temporal dysregulation of MPC lineage specification contributes to impaired regeneration.<sup>52</sup> Therefore, we hypothesized that an EV treatment strategy designed to enhance both proliferation and myogenic differentiation of age MPCs may enhance outcomes.

To test our hypothesis, we utilized a 3D bioengineered muscle aging model with the goal of identifying the optimal EV therapeutic strategy in a time-efficient and high-throughput way. Our recent study systematically characterized the muscle aging model and found that 3D aged muscle constructs recapitulated age-related declines in myofiber function and regeneration when compared to young muscle constructs. Freviously, we found that, while young muscle constructs showed increased MPC amplification 1 day post injury (DPI), increases in MPC number were only detected in aged muscle constructs until 7 DPI. More importantly, the aged muscle

constructs recapitulated the regenerative responses of aged muscles to different interventions, including EVs.<sup>53</sup>

Aged muscle constructs were prepared by culturing aged MPCs in a 3D hydrogel mixture of fibrin and Matrigel and maintained in a PDMS chamber containing two posts that provided physical anchors for attachment to induce the development of aligned myotubes (Figure 4A, S5A, S5B). After 14 days of myotube induction, muscle constructs produced twitch and tetanic contractions upon 1 and 40 Hz electric stimulation, respectively (Figure S5C). To evaluate muscle regeneration, we injured aged muscle constructs by treating the constructs with 0.4  $\mu$ M CTX for 5 h, as we previously described. S3

With the goal of enhancing both MPC proliferation and differentiation to maximize muscle regenerative responses, we designed two strategies to treat injured aged muscle constructs: 1) administration of a mixture consisting of 1/2 fEVs and 1/2 nEVs ((f+n)EVs); and 2) sequential administration first of fEVs to promote proliferation followed by nEVs to induce cell differentiation  $((f\rightarrow n)EVs)$ , as shown in Figure 4B. Injured muscle constructs without treatment were used as controls. Another two groups of injured constructs were treated with solely fEVs or nEVs, respectively, replicating the protocol we had performed in vivo (Figure S4). At 7 DPI, we evaluated muscle construct regeneration by quantifying myotube number, myotube size, and force recovery. Similar to our in vivo results (Figure S4), the regeneration of aged muscle constructs was not improved when muscle constructs were treated with only fEVs or nEVs (Figure 4C-G). Similarly, the mixture of fEVs and nEVs yielded no improvement in regeneration compared to control counterparts (Figure 4C-G). However, muscle functional recovery was significantly improved when muscle constructs were treated sequentially, first with fEVs and then nEVs (Figure 4F-G). This increase in force production was concomitant with an increased number, but not size, of regenerated myotubes in the muscle constructs (Figure 4D,E). Regenerative outcomes were also dependent on EV dose (Figure S6). Of note, the sequential administration of fEVs and nEVs from aged MPCs also promoted muscle construct regeneration (Figure S7), though the degree of improvement was lower than using young EVs (42% (aged EVs) vs 85% (young EVs) based on tetanic force data). This further highlights nanotopography as a robust platform to modulate EV function. Taken together, our results suggest that the sequential administration of fEVs then nEVs may be a promising approach for improving aged muscle regeneration.

Sequential Administration of fEVs and nEVs Promoted Aged Muscle Regeneration In Vivo. Lastly, we revisited our in vivo model and evaluated the physiological relevance of the combined fEV and nEV administration protocol tested in the aged muscle constructs. TA muscles of aged male mice were again injected with CTX to induce injury. One group of mice received intramuscular injections of a mixture of 1/2 fEVs and 1/2 nEVs at both 1 and 5 DPI. Another group of mice received intramuscular injections of fEVs at 1 DPI and nEVs at 5 DPI (Figure 5A). The time points were selected based on previous reports demonstrating that activated MPCs proliferate at 1–3 DPI and undergo myogenic differentiation from 5 DPI. <sup>54,55</sup> Injured TA muscles of young and aged male mice without EV treatment (PBS injection only) were used as controls. Myofiber regeneration and contractile force production of injured muscles were assessed at 12 DPI. While administration of a mixed population of fEVs

and nEVs improved myofiber regeneration and increased the size of regenerating myofibers compared to aged controls (Figure 5B,C), there was no improvement in functional recovery (Figure 5D,E). By comparison, TA muscles received sequential treatment of fEVs and nEVs displayed even greater improvements in regeneration and to levels comparable to the young mouse TA muscles, as evidenced by significantly increased myofiber size and contractile forces (Figure 5B–E).

To further characterize the effects of sequential EV treatment on muscle regeneration, we also evaluated the inflammation, cell proliferation, and cell apoptosis at the treated site of muscle injury. We observed no significant difference in inflammation or cell apoptosis following  $(f \rightarrow n)$ EV treatment (Figure S8, S9). However,  $(f \rightarrow n)$ EV-treated muscle did contain fewer proliferating cells than the aged control (Figure S10). Given that the number of proliferating cells increases during the early stages of regeneration and decreases as the regenerative cascade progresses, we interpret these findings to suggest that our sequential EV treatment strategy may have accelerated the overall regeneration progress of aged skeletal muscle.

#### **CONCLUSION**

The temporal regulation of MPC proliferation and differentiation is critical for skeletal muscle regeneration but is impaired with aging. EV administration is increasingly recognized as a promising therapeutic strategy to promote tissue regeneration. Given that EV therapeutic efficiency is highly impacted by cell culture conditions, in the present work, we utilized nanotopography to tune the therapeutic potential of MPC-derived EVs for aged muscle regeneration. We found that EVs released by young MPCs cultured on flat substrates (fEVs) or nanogratings (nEVs) elicited distinct effects on aged MPC behavior, with the fEVs promoting cell proliferation and nEVs driving myogenic differentiation. By leveraging the advantages of the 3D biomimetic muscle aging model, we optimized a protocol of sequential administration of fEVs followed by nEVs to enhance aged muscle regeneration. The beneficial effects of this sequential EV treatment strategy were further validated in vivo in aged skeletal muscle. Collectively, this study not only provides an effective approach to tune the therapeutic potential of EVs through extrinsic topographical cues but also emphasizes the importance of optimizing EV administration strategy for skeletal muscle regeneration.

Study Limitations. While our study demonstrated the promise of modulating EV therapeutic function by using nanotopographical cues, we only evaluated a single shape and dimension of nanotopography. Whether and how nanotopography shape and dimension influence EV function represents an interesting future direction. Furthermore, we collected EVs from the conditioned media of the cells cultured on PDMS substrates for 3 days. We chose this time since it was the time point at which we found differences in the influence of nanotopographical cues on MPC phenotype and function in vitro. Given that EV cargoes may also be influenced by cell culture time, <sup>28</sup> it is worth investigating the influence of cell culture time on EV therapeutic performance. Lastly, our in vivo experiments were based on aged male mice. The effects of EV administration on muscle regeneration of aged female mice remain to be investigated.

#### MATERIALS AND METHODS

Animals. C57BL/6 young (3–6 months) and aged (21–25 months) male mice were selected for inclusion in our study. We chose these age ranges because mice older than 3 months are generally sexually mature and because mice at 21–25 months of age display well-documented declines in skeletal muscle regeneration. All mice were received from the National Institute on Aging (NIA) rodent colony. All procedures were approved by the Institutional Animal Care and Use Committee of the University of Pittsburgh and Mass General Hospital. The animals were given access to food and water ad libitum

Cell Isolation. MPCs were isolated from young and aged mice based on a published protocol using a preplating technique. Briefly, forelimb and hindlimb muscle tissues were minced and digested using collagenase II and Dispase to collect all populations of cells. The cells were then cultured in a collagen-coated T-flask. After 24 h of culture, the media containing floating cells was transferred to a Matrigel-coated T175 flask and maintained for 2–3 days to allow MPC adhesion. The cells were cultured in growth media consisting of high glucose Dulbecco's Modified Eagle Medium (DMEM, Gibco, Grand Island, NY, USA), 20% fetal bovine serum (FBS, Gibco), 0.5% chicken embryo extract (CEE, USBiological, Salem, MA, USA), 5 ng/mL basic fibroblast growth factor (bFGF, Peprotech, Cranbury, NJ, USA), and 1% penicillin-streptomycin (Gibco).

PDMS Substrate Preparation and Cell Culture. PDMS nanogratings were prepared through soft lithographic approaches.<sup>33</sup> Briefly, a mixture of PDMS resin and curing agent (Sylgard 184 kit, Dow Corning, Midland, MI, USA) in a 10:1 w/w ratio was poured onto a silicon mold and cured at 70 °C for 4 h. PDMS flat substrates were prepared by pouring PDMS uncured mixture on Petri dishes and cured at 70 °C for 4 h. Before seeding cells, the PDMS substrate surfaces were hydrophilized by air plasma treatment and coated with fibronectin (50 μg/mL, MilliporeSigma, St. Louis, MO, USA) for at least 1 h.

MPCs were seeded on flat or nanograting substrates at the density of 5000 cells/cm² in the growth media. When evaluating myotube formation, cells were cultured in growth media overnight to allow adhesion, followed by culturing in differentiation media for 3 days. The differentiation media consists of high glucose DMEM (Gibco), 2% horse serum (Gibco), and 1% penicillin-streptomycin (Gibco).

Treatment of GW4869 and Pitstop2. MPCs were seeded on flat or nanograting substrates at the density of 5000 cells/cm<sup>2</sup> in the growth media. After overnight incubation, the cells were then cultured in differentiation media containing either 5  $\mu$ M GW4869 (MilliporeSigma) or 25  $\mu$ M Pitstop 2 (MilliporeSigma) for another 3 days.

Immunostaining. Cells or tissue sections were fixed with 2% paraformaldehyde (PFA, ThermoFisher Scientific, Waltham, MA, USA) for 10 min at room temperature, permeabilized and blocked using a PBS solution containing 0.03 g/mL BSA (ThermoFisher Scientific), 10% goat serum (Gibco), and 0.2% Triton-X 100 (Sigma-Aldrich) for 1 h. The samples were then incubated with primary antibody (in PBS solution with 5% goat serum) overnight at 4 °C, then incubated with secondary antibody (1:200) for 1 h at room temperature. Nuclei were stained with DAPI (1:500, Invitrogen, Waltham, MA, USA) for 5 min. F-actin was stained with Alexa Fluor 488 phalloidin (1:400, Invitrogen). Details regarding the antibody information and dilution are listed in Table S1. During staining, at least one sample was incubated with the secondary antibody but not the primary antibody. These were used as negative controls to rule out the influence of nonspecific secondary antibody binding. Fluorescent images were captured using a Zeiss-Axiovision microscope. The confocal images were captured using a Nikon Confocal Microscope. Image analysis was performed using ImageJ (https://imagej.nih.gov/ ij/) or Fiji (https://imagej.net/software/fiji/).

**Western Blotting.** Cells were lysed by using RIPA buffer containing protease inhibitor for 30 min on ice, and the obtained proteins were separated with a 4–12% Bis-Tris gel electrophoresis (Invitrogen) and then transferred to polyvinylidene difluoride (PVDF) membranes (EMD Millipore, Burlington, MA, USA). The

PVDF membranes were blocked with blocking buffer (LI-COR Biosciences, NE, USA) for 1 h at room temperature, blotted with primary antibodies at 4 °C overnight, and then incubated with fluorescent dye-conjugated secondary antibodies (LI-COR Biosciences) for 1 h at room temperature. Details about the antibodies and their dilution are listed in Table S1. Protein membrane images were acquired using LI-COR ODYSSEY CLx and LI-COR Image Studio Acquisition Software (LI-COR Biosciences). The quantification of protein band densitometry was analyzed by using ImageJ software. Full blots are presented in Figure S10.

EV Isolation and Characterization. For EV isolation, young MPCs seeded on flat or nanograting substrates were cultured in EVfree growth media for 3 days. EVs were isolated either by using the total exosome isolation reagent (ThermoFisher Scientific) by following the manufacturer's protocol, through ultracentrifugation, or using size-exclusion chromatography (SEC) columns (ICO-35, Izon Science, Medford, MA, USA). To isolate EVs through ultracentrifugation, the conditioned media were collected and centrifuged for 30 min at 3,000g, followed by centrifuging the supernatant at 100,000g (Beckman Coulter Optima L-90K Ultracentrifuge) at 4 °C for 70 min. The EV pellet was then resuspended in PBS. To isolate EVs using SEC columns, the conditioned media was centrifuged for 30 min at 3,000g to remove debris and concentrated to a volume of approximately 150  $\mu$ L using centrifugal filters (100 kDa, Amicon UFC910024). The concentrated media was then run through the SEC columns and the 1.25-2.25 mL fraction was collected. The size and concentration of EVs were measured by a NanoSight NS 300.

Raman Spectroscopy. For the Raman spectroscopy analysis of EVs, 8 mL of cultured media was concentrated with Amicon 3 kDa Centrifugal Filter Unit (Millipore, Merck KGaA, Darmstadt, Germany) to 1 mL. SEC was performed using qEV columns (Gen2, 70 nm, Izon Science, Christchurch, New Zealand) and Automatic Fraction Collector (AFC; Izon Science) following the manufacturer's instructions. Briefly, 2900  $\mu L$  of eluted buffer was discarded and 1600 µL of fractions containing EVs was retained. EVs from 4 samples were pooled together and then concentrated by ultracentrifugation (100,000g × 70 min, 4 °C, L7-65; Rotor SW60; Beckman Coulter, Brea, CA, USA). The concentrated EVs were analyzed by Raman spectroscopy (LabRAM, Horiba Jobin Yvon S.A.S. Lille, France) following a previously published protocol. 42,4 Briefly, 5  $\mu$ L of the concentrated EVs were laid on a calcium fluoride disk and acquisitions were performed in the spectral ranges 600-1800 cm<sup>-1</sup> and 2600–3200 cm<sup>-1</sup> with the following parameters: 532 nm laser line; 50× objective; grating 1800; 400  $\mu$ m entrance slit; 30 s of acquisition for 2 repetitions. Instrument calibration was done using a reference sample (Si) at 570.7 cm<sup>-1</sup> prior to running the experiment. Twenty-five spectra per sample were collected randomly at the border of the EV drops, spectra with no signal or saturated signals were not considered for the subsequent analysis. The spectra were analyzed using LabSpec6 (Horiba) software. Spectra were aligned, and the baseline was corrected using a fifth-order polynomial curve and normalized dividing by the data set maximum value. The average spectrum was calculated for both experimental groups. A preliminary comparison of spectra was performed by multivariate statistical analysis. Principal component analysis (PCA) was used to minimize the variables, followed by Linear Discriminant Analysis performed by using the first 10 Principal Components. Canonical variable scores obtained for the two groups were compared using a nonparametric Mann-Whitney test.

In-Well Western for EV Characterization. In-well western was performed to confirm EV purity. Briefly, 1 × 109 EVs isolated through ultracentrifugation or SEC were fixed in 2% PFA for 10 min, followed by washing with PBS once. EVs were then blocked in PBS solution containing 3% BSA for 1 h at room temperature. After washing twice with PBS solution, EVs were incubated with Alex Fluor 647-labeled CD81(ThermoFisher Scientific), GM130 (Santa Cruz, Dallas, TX, USA), or ALIX (Proteintech, Rosemont, IL, USA) overnight at 4 °C, followed by incubating with fluorescent dyeconjugated secondary antibody for 1 h at room temperature. EVs were

washed twice with PBS, resuspended in 150  $\mu$ L of PBS, and loaded to a 96-well plate. The fluorescent imaging was performed using LI-COR ODYSSEY CLx and LI-COR Image Studio Acquisition Software (LI-COR Biosciences). Young MPCs were used as the positive control for GM130.

**Aged Muscle Construct Preparation.** The preparation of aged muscle constructs was conducted by following our previous study. Si Briefly,  $2 \times 10^6$  cells were suspended in 71.2  $\mu$ L growth media followed by adding 0.8  $\mu$ L Thrombin (Millipore Sigma, 100 U/mL in PBS containing 0.1% bovine serum albumin), 20  $\mu$ L Matrigel (Corning), and 8  $\mu$ L Fibrinogen (MP Biomedicals, Solon, OH, USA). 85  $\mu$ L of the mixture of cells and hydrogels was then added to the sterilized PDMS frame and incubated for 25 min at 37 °C for gelation. Muscle constructs were cultured in the growth media containing 1.5 mg/mL 6-aminocaproic acid (ACA; Sigma-Aldrich) for 4 days, followed by culturing in differentiation media supplementing with 2 mg/mL ACA for another 14 days to induce myotube formation and construct maturation. The contractile (twitch and tetanic) forces were measured and analyzed as previously described. Si

**In Vitro EV Treatment.** For the EV uptake experiment, aged MPCs cultured on glass chamber slides (ibidi, Fitchburg, WI, USA) were treated with PKH-26-labeled EVs at the concentration of  $1 \times 10^9$  EVs/mL for 4 h in EV-free media. The cells were then fixed in 2% PFA and stained for phalloidin.

To evaluate cell proliferation, aged MPCs were cultured either on glass chamber slides (ibidi) for 24 h (for Ki-67 staining) in the presence of EVs or in 96-well plates for 72 h (for MTS assay). MTS assays were performed using a CellTiter 96 AQueous One Solution Cell Proliferation Assay based on the manufacturer's instruction. To evaluate cell differentiation, aged MPCs were cultured on glass chamber slides (ibidi) and treated with EVs for 3 days in EV-free differentiation media (2% EV-free FBS (Gibco) and 1% penicillinstreptomycin in high glucose DMEM). Cells were then stained for MHC (Abcam, Waltham, MA). Myotube number, length, fusion index, and maturation index were then evaluated. The myotube fusion index was defined as the percentage of nuclei inside the myotubes, while the maturation index was defined as the percentage of myotubes containing more than five nuclei. 56–58

For muscle construct regeneration assays, aged muscle constructs were first treated with CTX (0.4  $\mu$ M) for 5 h on a shaker at 37 °C to induce myotube fragmentation. After CTX treatment, muscle constructs were cultured in the EV-free differentiation media containing 1  $\times$  10<sup>8</sup> –5  $\times$  10<sup>9</sup> of fEVs and/or nEVs isolated from young or aged MPCs. The EV-containing media was changed every other day. Contractile force and regenerated myotubes of muscle constructs were evaluated at 7 DPI.

In Vivo Muscle Regeneration. Young or aged male mice received bilateral TA muscle injuries by intramuscular injections of 10  $\mu$ L CTX (1 mg/mL), as we previously described. <sup>51</sup> Animals were then randomly assigned to each group. For fEV or nEV treatment experiments, animals received  $10-15~\mu L$  bilateral intramuscular injections of  $1 \times 10^9$  fEVs or nEVs at 5 and 7 DPI. For combined EV treatment experiments, animals received 10-15 µL bilateral intramuscular EV injections at 1 and 5 DPI. In the mixed EV treatment group ((f+n)EVs), mouse TA muscles were injected with an EV mixture containing  $5 \times 10^8$  fEVs and  $5 \times 10^8$  nEVs (total EVs:  $1 \times$ 10<sup>9</sup>). In the sequential EV treatment group ( $(f \rightarrow n)EVs$ ), the mouse TA muscles were injected with fEVs  $(1 \times 10^9)$  and nEVs  $(1 \times 10^9)$  at 1 and 5 DPI, respectively. In the control group, the mouse TA muscles were injected with the same amount of PBS as the EV solution. In situ contractile testing was performed by a blinded investigator at 12-14 DPI based on our previously described protocol.<sup>59</sup> TA muscles were collected and cryo-sectioned for histological analysis of myofiber regeneration. Muscle sections were stained for laminin and imaged using a Nikon confocal microscope. The cross-sectional area of myofibers was then quantified using MyoVision software (version 1.0).60 TUNEL staining was performed using Click-iT Plus TUNEL assay (Invitrogen) by following the manufacturer's protocol.

**Statistical Analysis.** Data are presented as mean  $\pm$  standard error of the mean (SEM). The sample size was calculated a priori by GPower software (Version 3.1). A Shapiro-Wilk test was initially performed to check the data normality. When normality conditions were met, the statistical significance was analyzed based on the two-tailed Student t test or one-way analysis of variance (ANOVA) followed by Tukey's HSD (honestly significant difference) for two-group and multiple-group comparisons, respectively. Otherwise, groups were compared using a Mann—Whitney U test or non-parametric ANOVA with Dunn's multiple comparisons. The statistical analyses were performed using GraphPad Prism 9 or JMP Pro (version 16.0). Statistically significant differences were considered at a level of p < 0.05.

### **ASSOCIATED CONTENT**

## **Data Availability Statement**

The data are available for research purposes from the corresponding authors upon reasonable request.

## **Supporting Information**

The Supporting Information is available free of charge at https://pubs.acs.org/doi/10.1021/acsnano.3c02269.

Figure S1. Nanogratings promoted p38 MAPK expression and phosphorylation. Figure S2. In-well immunofluorescence western characterization of EVs. Figure S3. Proliferation of aged MPCs with or without EV treatment. Figure S4. Effects of fEV or nEV administration on aged muscle regeneration. Figure S5. Characterization of aged muscle constructs. Figure S6. Relative tetanic forces of injured aged muscle constructs treated with EVs at different doses. Figure S7. Relative tetanic forces of injured aged muscle constructs treated sequentially with fEVs and nEVs secreted by aged MPCs. Figure S8. The effects of in vivo sequential fEVs and nEVs administration on tissue inflammation. Figure S9. The effects of in vivo sequential fEVs and nEVs administration on cell apoptosis. Figure S10. The effects of in vivo sequential fEVs and nEVs administration on cell proliferation. Figure S11. Full blots of the Western blots performed in this study. Table S1. Information of primary antibodies used in this study. (PDF)

## **AUTHOR INFORMATION**

#### **Corresponding Authors**

Kai Wang — Discovery Center for Musculoskeletal Recovery, Schoen Adams Research Institute at Spaulding, Charlestown, Massachusetts 02129, United States; Department of Physical Medicine & Rehabilitation, Harvard Medical School, Boston, Massachusetts 02115, United States; Department of Physical Medicine & Rehabilitation, Spaulding Rehabilitation Hospital, Charlestown, Massachusetts 02129, United States; Department of Physical Medicine & Rehabilitation, University of Pittsburgh, Pittsburgh, Pennsylvania 15213, United States; orcid.org/0000-0001-8447-6177; Email: kwang36@mgh.harvard.edu

Fabrisia Ambrosio — Discovery Center for Musculoskeletal Recovery, Schoen Adams Research Institute at Spaulding, Charlestown, Massachusetts 02129, United States; Department of Physical Medicine & Rehabilitation, Harvard Medical School, Boston, Massachusetts 02115, United States; Department of Physical Medicine & Rehabilitation, Spaulding Rehabilitation Hospital, Charlestown, Massachusetts 02129, United States; Department of Physical Medicine & Rehabilitation, University of Pittsburgh, Pittsburgh, Pennsylvania 15213, United States; Email: fambrosio@mgh.harvard.edu

#### **Authors**

- Nolan Frey Department of Biological Sciences, Carnegie Mellon University, Pittsburgh, Pennsylvania 15213, United States
- Andres Garcia Department of Mechanical Engineering, Carnegie Mellon University, Pittsburgh, Pennsylvania 15213, United States; orcid.org/0000-0002-4822-202X
- Kun Man Department of Biomedical Engineering, University of North Texas, Denton, Texas 76207, United States; orcid.org/0000-0002-3764-3312
- Yong Yang Department of Biomedical Engineering, University of North Texas, Denton, Texas 76207, United States; orcid.org/0000-0003-4305-8029
- Alice Gualerzi IRCCS Fondazione Don Carlo Gnocchi ONLUS, Milan 20148, Italy; o orcid.org/0000-0003-2996-5714
- Zachary J. Clemens Department of Environmental and Occupational Health, University of Pittsburgh, Pittsburgh, Pennsylvania 15213, United States
- Marzia Bedoni IRCCS Fondazione Don Carlo Gnocchi ONLUS, Milan 20148, Italy
- Philip R. LeDuc Department of Biological Sciences,
  Department of Mechanical Engineering, Department of
  Computational Biology, Department of Biomedical
  Engineering, and Department of Electrical and Computer
  Engineering, Carnegie Mellon University, Pittsburgh,
  Pennsylvania 15213, United States

Complete contact information is available at: https://pubs.acs.org/10.1021/acsnano.3c02269

## Notes

The authors declare no competing financial interest.

## **ACKNOWLEDGMENTS**

This study was supported in part by NIA grants R01AG052978 (F.A.), R01AG061005 (F.A., P.L.), and R01AG066198-01 (F.A.). We gratefully acknowledge the Center for Biological Imaging at the University of Pittsburgh (National Institutes of Health grant 1S10OD019973).

## **REFERENCES**

- (1) Relaix, F.; Bencze, M.; Borok, M. J.; Der Vartanian, A.; Gattazzo, F.; Mademtzoglou, D.; Perez-Diaz, S.; Prola, A.; Reyes-Fernandez, P. C.; Rotini, A.; Taglietti Perspectives on skeletal muscle stem cells. *Nat. Commun.* **2021**, *12* (1). DOI: 10.1038/s41467-020-20760-6
- (2) Schmidt, M.; Schüler, S. C.; Hüttner, S. S.; von Eyss, B.; von Maltzahn, J. Adult stem cells at work: regenerating skeletal muscle. *Cell. Mol. Life Sci.* **2019**, *76*, 2559–2570.
- (3) Brack, A. S.; Conboy, I. M.; Conboy, M. J.; Shen, J.; Rando, T. A. A Temporal Switch from Notch to Wnt Signaling in Muscle Stem Cells Is Necessary for Normal Adult Myogenesis. *Cell Stem Cell* **2008**, 2 (1), 50–59.
- (4) Blau, H. M.; Cosgrove, B. D.; Ho, A. T. The central role of muscle stem cells in regenerative failure with aging. *Nature medicine* **2015**, 21 (8), 854–862.
- (5) Chakkalakal, J. V.; Jones, K. M.; Basson, M. A.; Brack, A. S. The aged niche disrupts muscle stem cell quiescence. *Nature* **2012**, 490 (7420), 355–360.
- (6) Blau, H. M. Cell therapies for muscular dystrophy. *N Engl J. Med.* **2008**, 359 (13), 1403–1405.

- (7) Hall, J. K.; Banks, G. B.; Chamberlain, J. S.; Olwin, B. B. Prevention of muscle aging by myofiber-associated satellite cell transplantation. *Sci. Transl. Med.* **2010**, *2* (57), 57ra83–57ra83.
- (8) Mahindran, E.; Law, J. X.; Ng, M. H.; Nordin, F. Mesenchymal Stem Cell Transplantation for the Treatment of Age-Related Musculoskeletal Frailty. *International Journal of Molecular Sciences* **2021**, 22 (19), 10542.
- (9) Motohashi, N.; Asakura, Y.; Asakura, A. Isolation, culture, and transplantation of muscle satellite cells. *JoVE* (*Journal of Visualized Experiments*) **2014**, *86*, No. e50846.
- (10) Gilbert, P. M.; Havenstrite, K. L.; Magnusson, K. E.; Sacco, A.; Leonardi, N. A.; Kraft, P.; Nguyen, N. K.; Thrun, S.; Lutolf, M. P.; Blau, H. M. Substrate elasticity regulates skeletal muscle stem cell self-renewal in culture. *Science* **2010**, 329 (5995), 1078–1081.
- (11) Wood, K. J.; Issa, F.; Hester, J. Understanding stem cell immunogenicity in therapeutic applications. *Trends in immunology* **2016**, 37 (1), 5–16.
- (12) Sun, H.; Pratt, R. E.; Hodgkinson, C. P.; Dzau, V. J. Sequential paracrine mechanisms are necessary for the therapeutic benefits of stem cell therapy. *American Journal of Physiology-Cell Physiology* **2020**, 319 (6), C1141–C1150.
- (13) Mirotsou, M.; Jayawardena, T. M.; Schmeckpeper, J.; Gnecchi, M.; Dzau, V. J. Paracrine mechanisms of stem cell reparative and regenerative actions in the heart. *Journal of molecular and cellular cardiology* **2011**, *50* (2), 280–289.
- (14) Wiklander, O. P.; Brennan, M. Á.; Lötvall, J.; Breakefield, X. O.; El Andaloussi, S. Advances in therapeutic applications of extracellular vesicles. *Sci. transl. Med.* **2019**, *11* (492), eaav8521.
- (15) Gurung, S.; Perocheau, D.; Touramanidou, L.; Baruteau, J. The exosome journey: From biogenesis to uptake and intracellular signalling. *Cell Commun. Signal.* **2021**, *19* (1), 1–19.
- (16) Turturici, G.; Tinnirello, R.; Sconzo, G.; Geraci, F. Extracellular membrane vesicles as a mechanism of cell-to-cell communication: advantages and disadvantages. *American Journal of Physiology-Cell Physiology* **2014**, *306* (7), C621–C633.
- (17) Casado-Diaz, A.; Quesada-Gomez, J. M.; Dorado, G., Extracellular Vesicles Derived From Mesenchymal Stem Cells (MSC) in Regenerative Medicine: Applications in Skin Wound Healing. Front. Bioeng. Biotechnol. 2020, 8. DOI: 10.3389/fbioe.2020.00146
- (18) Jin, Q. Q.; Li, P. L.; Yuan, K. Y.; Zhao, F.; Zhu, X. H.; Zhang, P. F.; Huang, Z. W. Extracellular vesicles derived from human dental pulp stem cells promote osteogenesis of adipose-derived stem cells via the MAPK pathway. *J. Tissue Eng.* **2020**, *11*, 204173142097556.
- (19) Choi, J. S.; Yoon, H. I.; Lee, K. S.; Choi, Y. C.; Yang, S. H.; Kim, I.-S.; Cho, Y. W. Exosomes from differentiating human skeletal muscle cells trigger myogenesis of stem cells and provide biochemical cues for skeletal muscle regeneration. *Journal of controlled release* **2016**, 222, 107–115.
- (20) Yates, A. G.; Pink, R. C.; Erdbrugger, U.; Siljander, P. R.-M.; Dellar, E. R.; Pantazi, P.; Akbar, N.; Cooke, W. R.; Vatish, M.; Dias-Neto, E.; Anthony, D. C.; Couch, Y. In sickness and in health: The functional role of extracellular vesicles in physiology and pathology in vivo: Part I: Health and Normal Physiology. *J. Extracellular Vesicle* 2022, 11 (1), No. e12151.
- (21) Chen, Y.; Yu, L. Extracellular vesicles: from bench to bedside. Curr. Med. 2022, 1 (1), 3.
- (22) Yang, Y.; Wang, K.; Gu, X.; Leong, K. W. Biophysical regulation of cell behavior—cross talk between substrate stiffness and nanotopography. *Engineering* **2017**, *3* (1), 36–54.
- (23) Dalby, M. J.; Gadegaard, N.; Oreffo, R. O. Harnessing nanotopography and integrin-matrix interactions to influence stem cell fate. *Nature materials* **2014**, *13* (6), 558–569.
- (24) Wang, K.; Man, K.; Liu, J.; Meckes, B.; Yang, Y. Dissecting Physical and Biochemical Effects in Nanotopographical Regulation of Cell Behavior. *ACS Nano* **2023**, *17* (3), 2124–2133.
- (25) Teo, B. K. K.; Wong, S. T.; Lim, C. K.; Kung, T. Y.; Yap, C. H.; Ramagopal, Y.; Romer, L. H.; Yim, E. K. Nanotopography modulates

- mechanotransduction of stem cells and induces differentiation through focal adhesion kinase. ACS Nano 2013, 7 (6), 4785–4798.
- (26) Tsui, J. H.; Janebodin, K.; Ieronimakis, N.; Yama, D. M.; Yang, H. S.; Chavanachat, R.; Hays, A. L.; Lee, H.; Reyes, M.; Kim, D.-H. Harnessing sphingosine-1-phosphate signaling and nanotopographical cues to regulate skeletal muscle maturation and vascularization. *ACS Nano* 2017, 11 (12), 11954–11968.
- (27) Nakayama, K. H.; Quarta, M.; Paine, P.; Alcazar, C.; Karakikes, I.; Garcia, V.; Abilez, O. J.; Calvo, N. S.; Simmons, C. S.; Rando, T. A.; Huang, N. F. Treatment of volumetric muscle loss in mice using nanofibrillar scaffolds enhances vascular organization and integration. *Commun. Biol.* **2019**, 2 (1), 170.
- (28) Ma, L.; Li, G.; Lei, J.; Song, Y.; Feng, X.; Tan, L.; Luo, R.; Liao, Z.; Shi, Y.; Zhang, W.; Liu, X.; Sheng, W.; Wu, S.; Yang, C. Nanotopography sequentially mediates human mesenchymal stem cell-derived small extracellular vesicles for enhancing osteogenesis. *ACS Nano* 2022, 16 (1), 415–430.
- (29) Ma, L.; Ke, W.; Liao, Z.; Feng, X.; Lei, J.; Wang, K.; Wang, B.; Li, G.; Luo, R.; Shi, Y.; Zhang, W.; Song, Y.; Sheng, W.; Yang, C. Small extracellular vesicles with nanomorphology memory promote osteogenesis. *Bioactive materials* **2022**, *17*, 425–438.
- (30) Xu, B.; Magli, A.; Anugrah, Y.; Koester, S. J.; Perlingeiro, R. C.; Shen, W. Nanotopography-responsive myotube alignment and orientation as a sensitive phenotypic biomarker for Duchenne muscular dystrophy. *Biomaterials* **2018**, *183*, 54–66.
- (31) Yang, H. S.; Ieronimakis, N.; Tsui, J. H.; Kim, H. N.; Suh, K.-Y.; Reyes, M.; Kim, D.-H. Nanopatterned muscle cell patches for enhanced myogenesis and dystrophin expression in a mouse model of muscular dystrophy. *Biomaterials* **2014**, 35 (5), 1478–1486.
- (32) Webster, M. T.; Manor, U.; Lippincott-Schwartz, J.; Fan, C.-M. Intravital Imaging Reveals Ghost Fibers as Architectural Units Guiding Myogenic Progenitors during Regeneration. *Cell Stem Cell* **2016**, *18* (2), 243–252.
- (33) Wang, K.; Bruce, A.; Mezan, R.; Kadiyala, A.; Wang, L.; Dawson, J.; Rojanasakul, Y.; Yang, Y. Nanotopographical modulation of cell function through nuclear deformation. *ACS Appl. Mater. Interfaces* **2016**, *8* (8), 5082–5092.
- (34) Song, L.; Wang, K.; Li, Y.; Yang, Y. Nanotopography promoted neuronal differentiation of human induced pluripotent stem cells. *Colloids Surf., B* **2016**, *148*, 49–58.
- (35) Martineau, L. C.; Gardiner, P. F. Insight into skeletal muscle mechanotransduction: MAPK activation is quantitatively related to tension. *Journal of applied physiology* **2001**, *91* (2), 693–702.
- (36) Zhan, M.; Jin, B.; Chen, S.-E.; Reecy, J. M.; Li, Y.-P. TACE release of TNF- $\alpha$  mediates mechanotransduction-induced activation of p38 MAPK and myogenesis. *Journal of cell science* **2007**, 120 (4), 692–701
- (37) Keren, A.; Tamir, Y.; Bengal, E. The p38 MAPK signaling pathway: a major regulator of skeletal muscle development. *Molecular and cellular endocrinology* **2006**, 252 (1–2), 224–230.
- (38) Padmanabhan, J.; Augelli, M. J.; Cheung, B.; Kinser, E. R.; Cleary, B.; Kumar, P.; Wang, R.; Sawyer, A. J.; Li, R.; Schwarz, U. D.; Schroers, J.; Kyriakides, T. R. Regulation of cell-cell fusion by nanotopography. *Sci. Rep.* **2016**, *6* (1), 1–9.
- (39) Jiang, N.; Xiang, L.; He, L.; Yang, G.; Zheng, J.; Wang, C.; Zhang, Y.; Wang, S.; Zhou, Y.; Sheu, T.-J.; Wu, J.; Chen, K.; Coelho, P. G.; Tovar, N. M.; Kim, S. H.; Chen, M.; Zhou, Y.-H.; Mao, J. J. Exosomes mediate epithelium—mesenchyme crosstalk in organ development. ACS Nano 2017, 11 (8), 7736–7746.
- (40) Horibe, S.; Tanahashi, T.; Kawauchi, S.; Murakami, Y.; Rikitake, Y. Mechanism of recipient cell-dependent differences in exosome uptake. *BMC Cancer* **2018**, *18* (1), 1–9.
- (41) Hanson, B.; Vorobieva, I.; Zheng, W.; Conceição, M.; Lomonosova, Y.; Mäger, I.; Puri, P. L.; El Andaloussi, S.; Wood, M. J.; Roberts, T. C. EV-mediated promotion of myogenic differentiation is dependent on dose, collection medium, and isolation method. *Molecular Therapy-Nucleic Acids* **2023**, *33*, 511–528.
- (42) Gualerzi, A.; Kooijmans, S. A. A.; Niada, S.; Picciolini, S.; Brini, A. T.; Camussi, G.; Bedoni, M. Raman spectroscopy as a quick tool to

- assess purity of extracellular vesicle preparations and predict their functionality. J. Extracellular Vesicle 2019, 8 (1), 1568780.
- (43) Gualerzi, A.; Niada, S.; Giannasi, C.; Picciolini, S.; Morasso, C.; Vanna, R.; Rossella, V.; Masserini, M.; Bedoni, M.; Ciceri, F.; Bernardo, M. E.; Brini, A. T.; Gramatica, F., Raman spectroscopy uncovers biochemical tissue-related features of extracellular vesicles from mesenchymal stromal cells. *Sci. Rep.* **2017**, 7 (1). DOI: 10.1038/s41598-017-10448-1
- (44) Movasaghi, Z.; Rehman, S.; Rehman, I. U. Raman spectroscopy of biological tissues. *Appl. Spectrosc. Rev.* **2007**, 42 (5), 493–541.
- (45) Tsimbouri, P. M.; McMurray, R. J.; Burgess, K. V.; Alakpa, E. V.; Reynolds, P. M.; Murawski, K.; Kingham, E.; Oreffo, R. O.; Gadegaard, N.; Dalby, M. J. Using nanotopography and metabolomics to identify biochemical effectors of multipotency. *ACS Nano* **2012**, *6* (11), 10239–10249.
- (46) Lu, C.-H.; Pedram, K.; Tsai, C.-T.; Jones, T., IV; Li, X.; Nakamoto, M. L.; Bertozzi, C. R.; Cui, B. Membrane curvature regulates the spatial distribution of bulky glycoproteins. *Nat. Commun.* **2022**, *13* (1), 3093.
- (47) Chakravarthy, M. V.; Davis, B. S.; Booth, F. W. IGF-I restores satellite cell proliferative potential in immobilized old skeletal muscle. *J. Appl. Physiol.* **2000**, 89 (4), 1365–1379.
- (48) García-Prat, L.; Sousa-Victor, P.; Muñoz-Cánoves, P. Functional dysregulation of stem cells during aging: a focus on skeletal muscle stem cells. *FEBS journal* **2013**, 280 (17), 4051–4062.
- (49) Tanaka, K.; Sato, K.; Yoshida, T.; Fukuda, T.; Hanamura, K.; Kojima, N.; Shirao, T.; Yanagawa, T.; Watanabe, H. Evidence for cell density affecting C2C12 myogenesis: possible regulation of myogenesis by cell–cell communication. *Muscle & nerve* **2011**, *44* (6), 968–977.
- (50) Arnold, L. L.; Cecchini, A.; Stark, D. A.; Ihnat, J.; Craigg, R. N.; Carter, A.; Zino, S.; Cornelison, D. EphA7 promotes myogenic differentiation via cell-cell contact. *Elife* **2020**, *9*, No. e53689.
- (51) Sahu, A.; Clemens, Z. J.; Shinde, S. N.; Sivakumar, S.; Pius, A.; Bhatia, A.; Picciolini, S.; Carlomagno, C.; Gualerzi, A.; Bedoni, M.; Van Houten, B.; Lovalekar, M.; Fitz, N. F.; Lefterov, I.; Barchowsky, A.; Koldamova, R.; Ambrosio, F. Regulation of aged skeletal muscle regeneration by circulating extracellular vesicles. *Nat. Aging* **2021**, *1* (12), 1148–1161.
- (52) Brack, A. S.; Conboy, I. M.; Conboy, M. J.; Shen, J.; Rando, T. A. A temporal switch from notch to Wnt signaling in muscle stem cells is necessary for normal adult myogenesis. *Cell Stem Cell* **2008**, 2 (1), 50–9.
- (53) Wang, K.; Smith, S. H.; Iijima, H.; Hettinger, Z. R.; Mallepally, A.; Shroff, S. G.; Ambrosio, F. Bioengineered 3D Skeletal Muscle Model Reveals Complement 4b as a Cell-Autonomous Mechanism of Impaired Regeneration with Aging. *Adv. Mater.* **2023**, *35*, 2207443.
- (54) Shi, X.; Garry, D. J. Muscle stem cells in development, regeneration, and disease. *Genes & development* **2006**, 20 (13), 1692–1708.
- (55) Chazaud, B. Inflammation and skeletal muscle regeneration: leave it to the macrophages! *Trends in immunology* **2020**, *41* (6), 481–492
- (56) Kim, J.; Leem, J.; Kim, H. N.; Kang, P.; Choi, J.; Haque, M. F.; Kang, D.; Nam, S. Uniaxially crumpled graphene as a platform for guided myotube formation. *Microsystems Nanoeng.* **2019**, *S* (1), 53.
- (57) Bajaj, P.; Reddy, B., Jr; Millet, L.; Wei, C.; Zorlutuna, P.; Bao, G.; Bashir, R. Patterning the differentiation of C2C12 skeletal myoblasts. *Integrative Biology* **2011**, 3 (9), 897–909.
- (58) Sun, Y.; Ge, Y.; Drnevich, J.; Zhao, Y.; Band, M.; Chen, J. Mammalian target of rapamycin regulates miRNA-1 and follistatin in skeletal myogenesis. *J. Cell Biol.* **2010**, *189* (7), 1157–1169.
- (59) Clemens, Z.; Sivakumar, S.; Pius, A.; Sahu, A.; Shinde, S.; Mamiya, H.; Luketich, N.; Cui, J.; Dixit, P.; Hoeck, J. D; Kreuz, S.; Franti, M.; Barchowsky, A.; Ambrosio, F. The biphasic and age-dependent impact of klotho on hallmarks of aging and skeletal muscle function. *Elife* **2021**, *10*, No. e61138.
- (60) Wen, Y.; Murach, K. A.; Vechetti, I. J., Jr; Fry, C. S.; Vickery, C.; Peterson, C. A.; McCarthy, J. J.; Campbell, K. S. MyoVision:

software for automated high-content analysis of skeletal muscle immunohistochemistry. *J. Appl. Physiol.* **2018**, *124* (1), 40–51.